PERGAMON

International Journal of Solids and Structures 38 (2001) 3251–3262

INTERNATIONAL JOURNAL OF SOLIDS and STRUCTURES

www.elsevier.com/locate/ijsolstr

Elastic–plastic mode-II fracture of adhesive joints

Q.D. Yang [a], M.D. Thouless [a,b,*], S.M. Ward [c]

[a] *Department of Mechanical Engineering and Applied Mechanics, University of Michigan, Ann Arbor, MI 48109-2125, USA*
[b] *Department of Materials Science and Engineering, University of Michigan, Ann Arbor, MI 48109-2125, USA*
[c] *Scientific Research Laboratories, Ford Motor Company, Dearborn, MI 48121, USA*

Received 10 December 1999; in revised form 8 May 2000

Abstract

A numerical study of the elastic–plastic mode-II fracture of adhesive joints is presented in this paper. A traction–separation law was used to simulate the mode-II interfacial fracture of adhesively bonded end-notched flexure (ENF) specimens loaded in three-point bending, with extensive plastic deformation accompanying failure. The fracture parameters for the traction–separation law were determined by comparing the numerical and experimental results for one particular geometry. These parameters were then used without further modification to simulate the fracture of other ENF specimens with different geometries. It was found that the numerical predictions for the loads and deformation were in excellent agreement with the corresponding experimental results. © 2001 Elsevier Science Ltd. All rights reserved.

Keywords: Adhesive joints; Fracture; Plasticity; Numerical modeling; Mechanical testing

1. Introduction

Joining two materials by a third phase is of long-standing interest in a variety of industrial and technological applications, including traditional adhesive bonding, brazing and soldering, and composite materials. For elastic adhesive joints, in which the deformation of the adherends is dominated by elasticity during the fracture process, the conditions for fracture can be predicted using linear-elastic fracture mechanics (LEFM). A substantial amount of work has been done in this area, and a detailed review of the appropriate mechanics has been given by Hutchinson and Suo (1992). However, the development of suitable analyses for the fracture of adhesive joints where the adherends deform plastically during the fracture process still remains incomplete because of the complications caused by the coupling between macroscopic plasticity in the adherends and the actual fracture process.

It has been demonstrated that the use of a traction–separation relation to characterize the fracture process is a very promising technique to deal with coupled plasticity and fracture (Hutchinson and Evans, 2000). A number of groups (Needleman, 1987, 1997; Tvergaard and Hutchinson, 1992, 1993, 1994; Wei and

* Corresponding author. Address: Department of Mechanical Engineering and Applied Mechanics, University of Michigan, Ann Arbor, MI 48109-2125, USA.
E-mail address: thouless@engin.umich.edu (M.D. Thouless).

0020-7683/01/$ - see front matter
PII: S0020-7683(00)00221-3

Hutchinson, 1997, 1998) have demonstrated that toughness is not the only controlling parameter when plasticity accompanies fracture: the cohesive stresses exerted at the crack tip also play a very important role. Fracture can be simulated by using an embedded-process-zone (or cohesive-zone) model in which the toughness and peak cohesive stress are used as the two major parameters characterizing the fracture process. By incorporating such a model into nonlinear finite-element analyses which account for plasticity in the surrounding materials, the energy dissipated by plasticity can be separated from that absorbed during the decohesion process along the crack plane.

The present work is motivated by the authors' attempt to establish a general modeling approach to obtain quantitative predictions for the fracture of adhesive joints that are deforming plastically. The core of this approach is to use a cohesive-zone model to mimic the role that the adhesive layer plays during the deformation and fracture of the joints. The interfacial toughness and cohesive stresses are incorporated in the traction–separation law of cohesive-zone elements that interact with the surrounding material. By doing this, the energy associated with fracture is completely separated out from the energy dissipated by gross plasticity in adherends. This approach has been successfully used to predict the mode-I fracture of various adhesive joints failing with extensive plastic deformation (Yang et al., 1999, 2000). An experimental procedure for determining the parameters of a suitable cohesive-zone model was proposed in these studies, and it was shown that numerical predictions based on these parameters were in excellent agreement with experimental results. While these studies demonstrated the success of the approach for mode-I fracture, establishing a general framework requires an understanding of mixed-mode fracture. As a first step towards this goal, a study of pure mode-II fracture is described here. An extension to the general mixed-mode case, based on this work and the earlier mode-I studies, has recently been developed (Yang and Thouless, 2000).

Three-point bending of adhesively bonded, end-notched flexure (ENF) specimens (Fig. 1) was chosen to provide the mode-II geometry. Stable crack growth occurs before the crack reaches the loading point in this type of specimen, and it provides an ideal case study for mode-II fracture. Furthermore, the test has previously been used to evaluate the mode-II fracture toughness of elastic adhesive joints based on LEFM concepts (Barret and Foschi, 1977; Chai, 1988). Chiang and Chai (1994) studied the plasticity in the adhesive layer near the static crack tip of elastic ENF adhesive joints using large-strain finite-element analyses. The deformation of the adhesive layer in the crack-tip region is essentially dominated by shear (with some compressive normal stresses at the crack tip). However, only elastically deforming adherends were considered in these earlier studies. When plasticity occurs, additional complications arise not only from the coupling effects between the fracture process and plasticity in adherends, but also from the geometric nonlinearities caused by large deformations and rotations of the specimens. Therefore, a full nonlinear numerical analysis incorporating an appropriate cohesive-zone model is necessary for modeling the fracture of such joints.

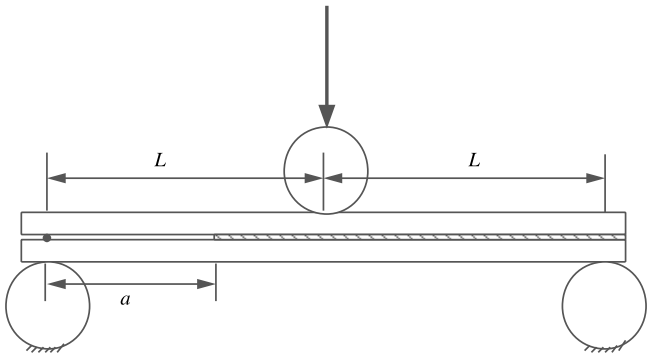

Fig. 1. Test configuration of an ENF specimen. The span, $2L$, is 60 mm, and the initial crack length, a, is 20 mm.

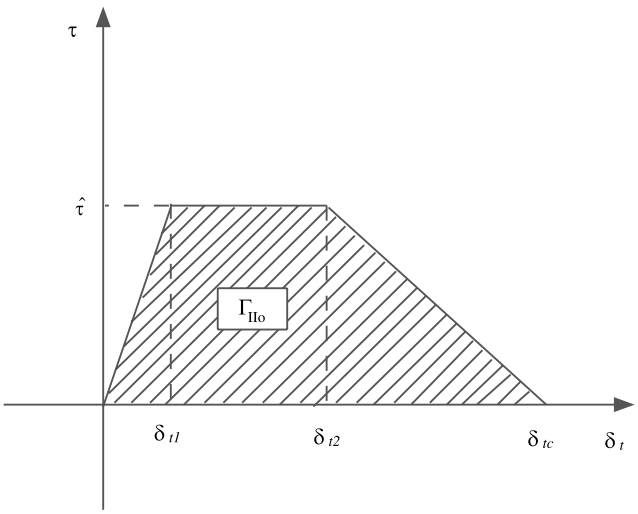

Fig. 2. The traction–separation law used in the numerical analyses. It is characterized by a work of separation per unit area, Γ_{IIo}, a peak shear stress, $\hat{\tau}$, and two shape parameters $\delta_{\mathrm{t1}}/\delta_{\mathrm{tc}}$ and $\delta_{\mathrm{t2}}/\delta_{\mathrm{tc}}$.

In this paper, a mode-II fracture problem is analyzed by adapting the technique previously used with success to model mode-I fracture (Yang et al., 1999). As shown in Fig. 2, the shear traction–separation relationship of a mode-II cohesive zone is characterized by Γ_{IIo}, the work of separation per unit area of crack growth (equal to the area under the curve), the peak shear stress supported by the bonding tractions, $\hat{\tau}$, and two shape parameters $\delta_{\mathrm{t1}}/\delta_{\mathrm{tc}}$ and $\delta_{\mathrm{t2}}/\delta_{\mathrm{tc}}$. Numerical experiments confirmed that Γ_{IIo} and $\hat{\tau}$ are the two key parameters that dominate the numerical simulations; the two shape parameters are less important. Therefore, in the work that follows, the two key parameters are first determined and then used to predict fracture. Comparisons between the numerical predictions and the experimental observations of crack propagation, deformation and fracture are used to validate the numerical technique.

2. Experiments

2.1. Torsion test of adhesively bonded butt joints

Torsion tests of adhesively bonded butt joints were conducted to obtain the shear properties of an adhesive layer (XD4600, from Ciba Specialty Chemicals) with a bond-line thickness of 0.25 mm. This is identical to the thickness used subsequently for the ENF specimens. This is essential because it is expected that the shear properties of adhesive layers depend upon the bond-line thickness (Chai, 1993). The butt joint was made of two solid aluminum cylindrical rods with a diameter of 12.7 mm (see the inset of Fig. 3(a)). The two rods were bonded together by the adhesive and carefully aligned by clamping them to a V-box during curing. The bond-line thickness was controlled by using uniform-sized silica spheres with a diameter of 0.25 mm as spacers. Subsequent measurements confirmed that the actual thickness was indeed 0.25 mm after the specimens were cured.

The shear test was performed on a torsion testing machine with a loading rate of 0.05 rad min^{-1}. The gauge length of the sample was 98 mm. In addition, an aluminum rod cut from the same batch and with the same gauge length was tested independently so that the elastic strain in the aluminum rods could be

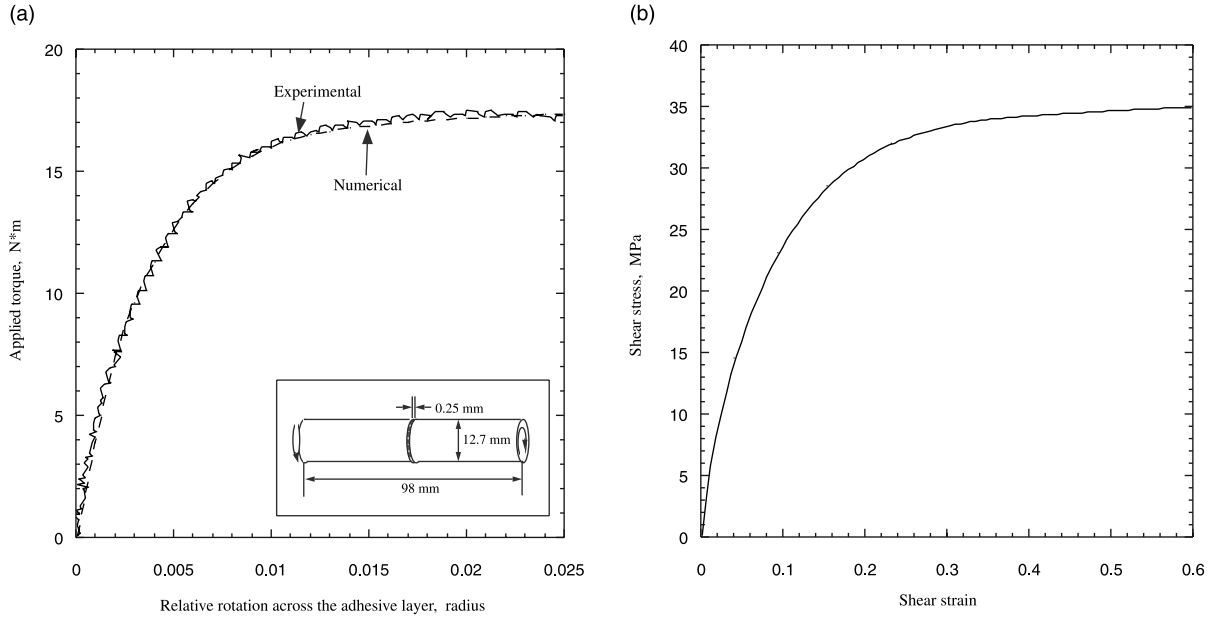

Fig. 3. (a) Experimental curve of applied torque *versus* relative rotation across the adhesive layer of butt joints (—). Also shown in this figure is the numerical results predicted by the constitutive properties shown in (b) (– – –). (b) Constitutive properties of the adhesive XD4600 backed out from the torsion test of adhesively bonded butt joints.

eliminated from the butt-joint test data. Curves of applied torque against rotation were recorded. After subtraction of the elastic rotation in the aluminum rods, a curve of applied torque versus relative rotation angle across the adhesive layer was obtained. This is shown as a solid line in Fig. 3(a). A numerical analysis using ABAQUS (5.8) with axisymmetric elements was performed to back out the shear stress–strain curve of the adhesive. The resultant curve is shown in Fig. 3(b). The results of the numerical simulation of the torsion test based upon this constitutive relation are shown as a dashed line in Fig. 3(a). The shear stress–strain curve for the adhesive given in Fig. 3(b) provided guidance in the subsequent determination of the mode-II fracture parameters used in the cohesive-zone model.

2.2. Three-point bending test of adhesively bonded end-notched flexure specimens

ENF specimens were fabricated using 20 mm wide coupons cut from aluminum sheets (5754 alloy from Alcan Rolled Products Company) of different thicknesses varying between 1.6 and 3.0 mm. The true stress–strain curve of the aluminum, which is essential for the numerical simulation to be introduced in next section, was obtained from standard uniaxial tensile tests and is shown in Fig. 4. The coupons were bonded by a layer of the commercial adhesive XD4600. The adhesive layer was kept at a uniform thickness of 0.25 mm using silica spheres as spacers. An initial crack along one of the adhesive/aluminum interfaces was introduced by inserting a strip of Teflon® tape into the interface before applying the adhesive. After curing, any excess adhesive was removed by careful filing and polishing of the specimen edges. To facilitate experimental observations, straight lines were cut vertically across the bond-lines using a sharp razor.

The specimens were placed over a test fixture consisting of two supporting cylinders. A third cylinder connected to the load cell of a tensile machine was used to bend the sample at its mid-point (Fig. 1). The span between the two supporting cylinders was 60 mm, and the initial crack length was 20 mm. To reduce

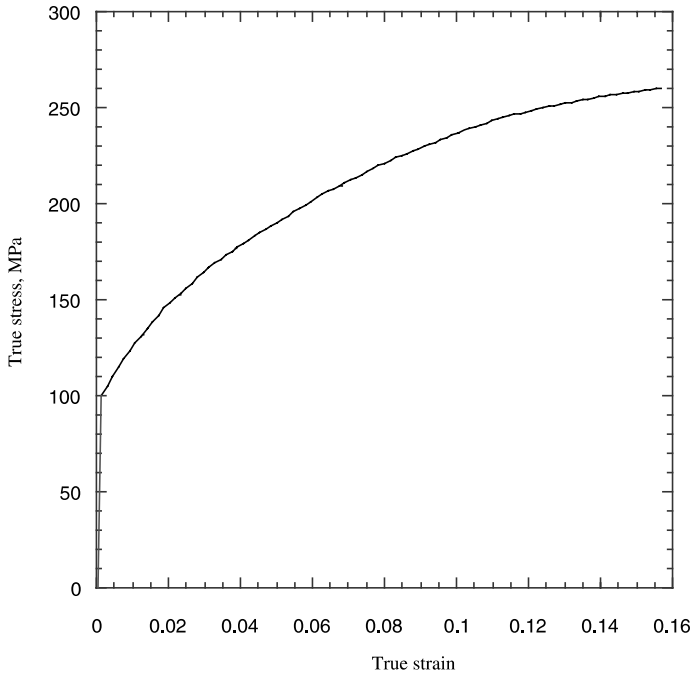

Fig. 4. The true stress–strain relation of the adherend material (5754 aluminum alloy).

possible frictional effects along the cracked surfaces, a glass fiber with a diameter of 0.4 mm was inserted as a spacer between the adherends at the crack mouth. The force and relative displacement between the center loading point and the supports were recorded as the specimens were deformed. The deflection measurements were made using a high-resolution CCD camera. This camera was also used to monitor the crack propagation and the deformation of the adhesive layer near the crack tip. A series of tests were performed for each thickness of aluminum. Each test was performed at room temperature, with a cross-head velocity of 2 mm min^{-1}. [1]

For all the specimens tested in this paper, the fracture was purely interfacial and the crack propagated along the interface between the adhesive layer and the compressive adherend. [2] The deformation of a 2.3 mm thick specimen immediately after the crack began to grow is shown in Fig. 5(a), and a magnified view of the crack-tip region is shown in Fig. 5(b). Fig. 5(a) indicates the extent of frictional sliding between the sample and the supports. The lines at the ends of the sample indicate the initial location of the contact points between the supports and the sample. The scribe marks in Fig. 5(b) show that the nominal shear strain across the bond line is about 40% at a distance approximately twice the adhesive thickness ahead of the crack tip. An even larger local strain is expected in the immediate vicinity of the crack tip, as also observed by Chai (1992). The full extent of the plastic zone, measured from the crack tip to the farthest point ahead of the tip which shows visible straining, was about 20 times the bond-line thickness.

[1] Experimental results show that there is no discernable difference between the load–displacement curves of samples tested at displacement rates of 0.2 and 200 mm min^{-1}.

[2] The crack always kinked into the interface immediately after it started to grow even if it was initiated at the mid-thickness of the adhesive layer.

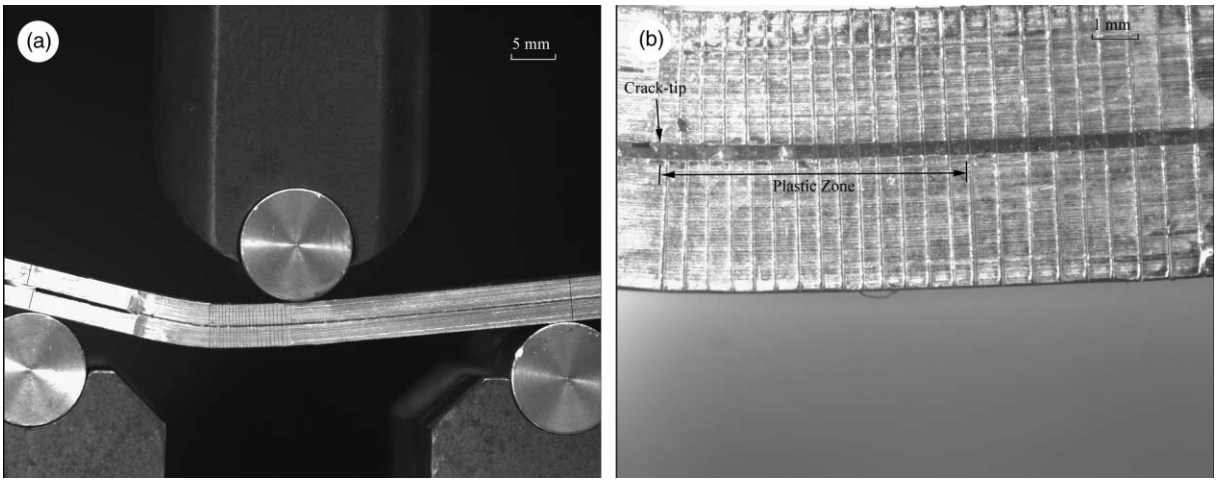

Fig. 5. (a) Micrograph of a deformed 2.3 mm thick ENF sample at the point at which the crack has just begun to grow. (b) A magnified view of the deformations in the vicinity of the crack tip.

3. Numerical simulations and comparisons to experimental results

Numerical calculations were performed to simulate the three-point bending tests. These calculations incorporated a cohesive-zone model within elastic–plastic finite-element calculations using the ABAQUS code (version 5.8). Except for the contact regions between the glass fiber and the adherends, where three-point elements were used in order to obtain a finer mesh, four-point bi-linear elements were used for the adherends. Reduced integration was used for all these elements in order to prevent possible shear-locking effects. Large-strain and large-rotation conditions were considered, with the von Mises yield criterion and an isotropic strain-hardening model being used to simulate the mechanical behavior of the adherends. Two-dimensional (2-D) analyses were used for the sake of numerical efficiency. It should be noted that plane-stress elements provided a better approximation to this geometry than plane-strain elements. Since this is not an obvious point, a more detailed discussion is given in Appendix A. Another important feature of this study was the use of contact elements to simulate the sliding between the supporting cylinders and the adherends, and between the glass fiber and the adherends. As can be seen from Fig. 5(a), there was fairly extensive sliding between the supporting cylinders and the adherends; this resulted in a decrease in the effective span length as the specimens deformed. Numerical experiments showed that failure to use contact elements between the supporting cylinders and adherends could result in as much as a 15% reduction in the predicted load. Therefore, it was deemed essential to use contact elements to allow the modeling of the sliding between the supporting cylinders and adherends, and between the glass fiber (spacer) and adherends.

In the numerical calculations, the adhesive layer was replaced by user-defined elements that simulated the appropriate traction–separation relationship of a mode-II cohesive-zone model. As described earlier, the work of separation per unit area, Γ_{IIo}, and the peak shear stress supported by the interface, $\hat{\tau}$, are the most important parameters that need to be determined for such a model. Systematic numerical experiments confirmed that the two shape parameters are less important, and they were chosen to be constants of $\delta_{\mathrm{t1}}/\delta_{\mathrm{tc}} = 0.15$ and $\delta_{\mathrm{t2}}/\delta_{\mathrm{tc}} = 0.5$ for all the simulations. The critical shear displacement, δ_{tc}, is fixed by the choice of the shape parameters, Γ_{IIo} and $\hat{\tau}$, since $\Gamma_{\mathrm{IIo}} = 0.5\hat{\tau}(\delta_{\mathrm{tc}} - \delta_{\mathrm{t1}} + \delta_{\mathrm{t2}})$.

The three-point bending tests showed that the local strain in crack-tip region was at least 40%. Therefore, it is evident from Fig. 3(b) that the peak shear stress can be taken as $\hat{\tau} = 35$ MPa. The mode-II joint toughness, Γ_{IIo} was then determined to be 5.4 kJ m^{-2} by using different values of Γ_{IIo} to predict load–

deflection curves for the 2.3 mm specimen, and finding the best fit to the associated experimental results. The resultant curve using these two parameters is shown in Fig. 6 together with a typical experimental curve. The oscillation in the numerical curve is caused by the difficult convergence procedure for the contact elements between the glass fiber and the adherends. The maximum loads in both the experimental and numerical curves correspond to the points at which the crack began to grow. The crack was observed to propagate steadily as the displacement was increased, but under a gradually decreasing load. It can be seen that the numerical calculation does an excellent job of reproducing the entire deformation history both before and after the beginning of crack growth. As a contrast to the numerical calculations using cohesive-zone elements, the results of a finite-element calculation using the continuum properties of the adhesive with no failure criterion are superimposed on Fig. 6. While such a calculation captures the deformation behavior until the crack begins to grow, the absence of a failure criterion renders it invalid after this point. However, the comparison shows that, in this particular case, the cohesive tractions are basically mimicking the deformations of the adhesive layer.

After being validated using the 2.3 mm thick samples, these values of $\hat{\tau} = 35$ MPa and $\Gamma_{\mathrm{IIo}} = 5.4\ \mathrm{kJ\,m^{-2}}$ were then used without any further modification to simulate the fracture of other specimens with different thicknesses of the aluminum. The numerical predictions for the applied loads and deflections are shown as solid lines in Fig. 7. The shaded areas in this figure indicate the ranges of the corresponding experimental data. The numerical results are in excellent agreement with the experimental results; they not only reproduce the magnitudes of the forces, but also capture some of the nuances of the shapes of the load–deflection curves. However, since plane-stress conditions were assumed in all the simulations, it is not surprising to see that the numerical results are closer to the lower bounds of the experimental data.

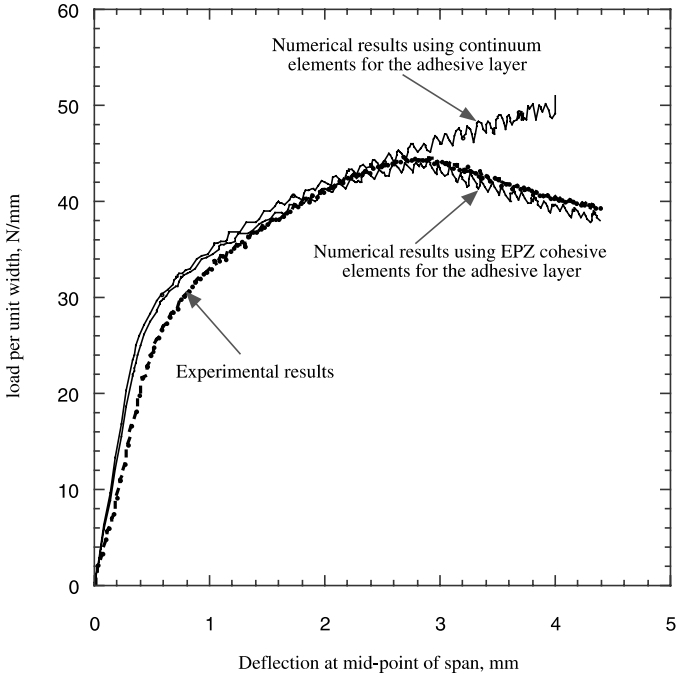

Fig. 6. Load (per unit width) for a 2.3 mm thick ENF specimen plotted as a function of the deflection at the mid-point of span. Three curves are compared: (i) experimental data, (ii) numerical results of a cohesive-zone model with $\hat{\tau} = 35$ MPa and $\Gamma_{\mathrm{IIo}} = 5.4\ \mathrm{kJ\,m^{-2}}$, and (iii) numerical results using a continuum model for the adhesive layer with no failure criterion.

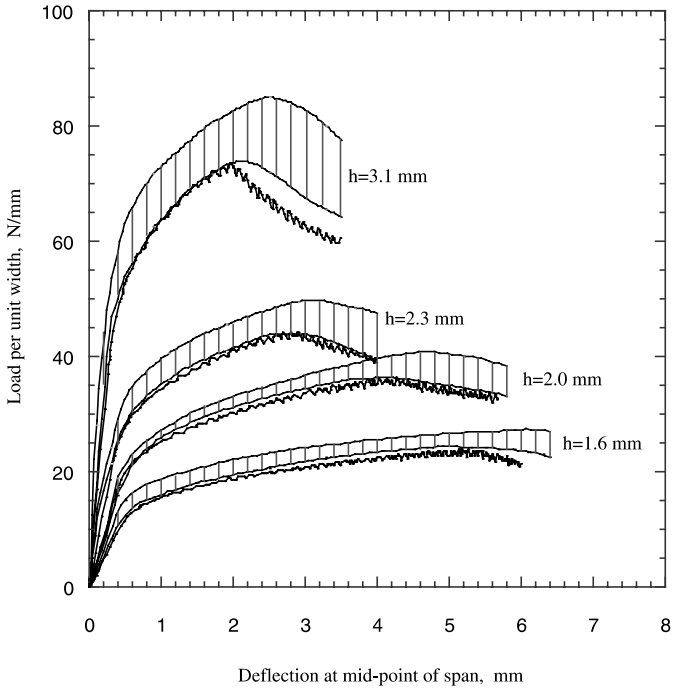

Fig. 7. Load (per unit width) plotted as a function of the deflection at the mid-point of the span for 1.6, 2.0, 2.3 and 3.0 mm thick, ENF specimens. The shaded areas show the range of experimental results. The solid lines show the results of numerical calculations with $\hat{\tau} = 35$ MPa and $\Gamma_{\mathrm{IIo}} = 5.4\ \mathrm{kJ\,m^{-2}}$.

The numerical prediction for the global deformation of a 2.3 mm thick specimen at the point when the crack begins to grow is shown in Fig. 8(a). A magnified view of the deformation and shear stress distribution near the crack tip is shown in Fig. 8(b). A comparison between these numerical predictions and the experimentally observed deformation (Fig. 5(a)) shows excellent agreement between the two. The predicted size of the plastic zone can be inferred from the extent of the shear deformation shown in Fig. 8(b); at approximately 20 times the bond-line thickness. This again agrees with the experimental observations (Fig. 5(b)).

4. Discussion

The pure mode-II interfacial toughness of the joint ($\Gamma_{\mathrm{IIo}} = 5.4\ \mathrm{kJ\,m^{-2}}$) is much higher than the associated *interfacial* mode-I value of $\Gamma_{\mathrm{Io}} = 1.0\ \mathrm{kJ\,m^{-2}}$ (with a peak normal cohesive stress $\hat{\sigma} = 60$ MPa), which was determined from wedge-induced fracture tests of double-cantilever beams bonded by an identical thickness of the adhesive (Yang and Thouless, 2000). [3] This demonstrates that the fracture is highly mode-dependent. Similar results were also observed by Chai in his systematic studies of the fracture of elastic adhesive joints (Chai, 1988, 1992). These studies showed that, except for extremely thin adhesive layers (<10 μm), the typical value of Γ_{IIo} was about an order of magnitude higher than the corresponding Γ_{Io} value. A major contribution to the high value of Γ_{IIo} is the higher capability of the adhesive layer to deform

[3] The value for Γ_{Io} quoted here is for *interfacial* failure. A value of Γ_{Io} $\mathrm{kJ\,m^{-2}}$ and $\hat{\sigma} = 100$ MPa was found for mode-I fracture within the adhesive layer (Yang et al., 1999).

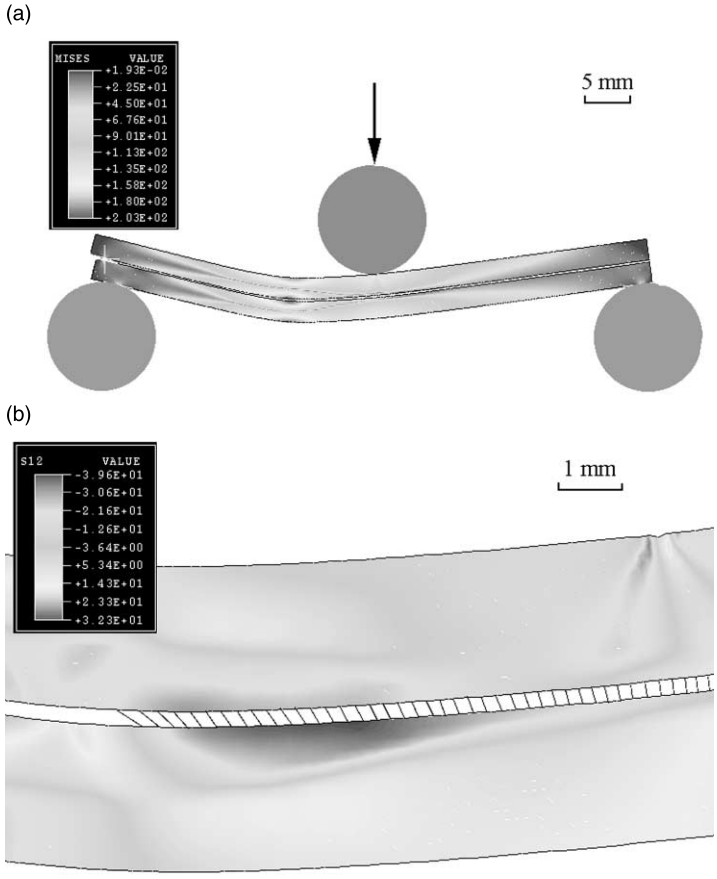

Fig. 8. (a) Numerical predictions for the deformation and the von Mises stress distribution in a 2.3 mm ENF sample at the point at which the crack has just begun to grow. (b) Numerical predictions for the distribution of shear stresses and for the shear displacements across the interface.

plastically in response to shear. In the interfacial mode-I fracture tests, the maximum tensile strain across the adhesive layer before fracture was observed to be only about 8%. The maximum shear strain observed in the torsion tests of the butt joints was about 60% (Fig. 3(b)). Therefore, much more energy is dissipated in the adhesive layer under mode-II loading than under mode-I loading. A rough estimate for the values of the mode-I and mode-II toughnesses can be obtained from the product of the critical displacements and cohesive stresses. For a 0.25 mm thick adhesive layer, the data given above would indicate a mode-I toughness of about 1 $kJ\,m^{-2}$ and a mode-II toughness of about 5 $kJ\,m^{-2}$. The large difference in the cohesive-zone parameters for mode-I fracture and mode-II fracture emphasizes the need for mode-dependent traction–separation relations to analyze mixed-mode fracture. This work has now been completed and will appear elsewhere (Yang and Thouless, 2000).

5. Conclusions

A pure mode-II cohesive-zone model has been used to simulate the elastic–plastic fracture of adhesively bonded, ENF specimens loaded by three-point bending. The fracture parameters of the model were

determined by matching the numerical results with the associated experimental results. These parameters were then used without any further modifications to predict the fracture of other adhesive joints with different thicknesses of adherends. The numerical predictions were in excellent agreement with the associated experimental results. Therefore, it has been demonstrated that it is possible to predict the loads associated with crack growth, and to model the entire deformation history of plastically deforming adhesive joints loaded in shear.

Acknowledgements

This work was supported by NSF Grant CMS-9624452 and Ford Motor Company. The authors would also like to express their appreciation to Prof. A. Waas and Mr. C.S. Yerramalli in the Department of Aerospace Engineering of University of Michigan for their help in the torsion test.

Appendix A

While a full 3-D calculation is required for a rigorous analysis of this problem, a 2-D approximation was used in the interests of numerical efficiency. *Plane-stress* elements were used in these calculations despite the fact that, at first glance, the samples might appear to be under plane-strain conditions. The reason that plane-stress elements proved to be more useful in this particular study is that the adhesive layer is much more compliant than the aluminum adherends, and does not provide the constraint necessary for plane-strain deformation of the specimen. To demonstrate this point, a three-point bend test was performed on an adhesive joint made from 2.0 mm thick aluminum coupons with no pre-crack. Fig. 9 shows the deformation in both the adherends and the adhesive. The relative displacements between the upper and lower beams, which result from shear deformation in the adhesive layer, are clearly seen in this figure. These displacements allow the two beams to deform in a relatively "independent" fashion – different from the predictions of simple beam theory. The stiffness of the composite beam is much lower than that of a solid beam with the same thickness.

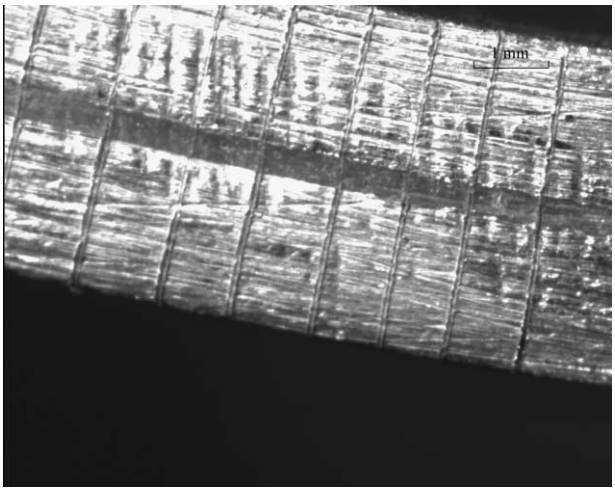

Fig. 9. The relative deformation across the adhesive layer in an adhesively bonded beam made with 2.0 mm thick aluminum adherends and tested in three-point bending. The span was 60 mm between the outside supports. (The shear displacements disappeared at the central loading point to the right of the figure.)

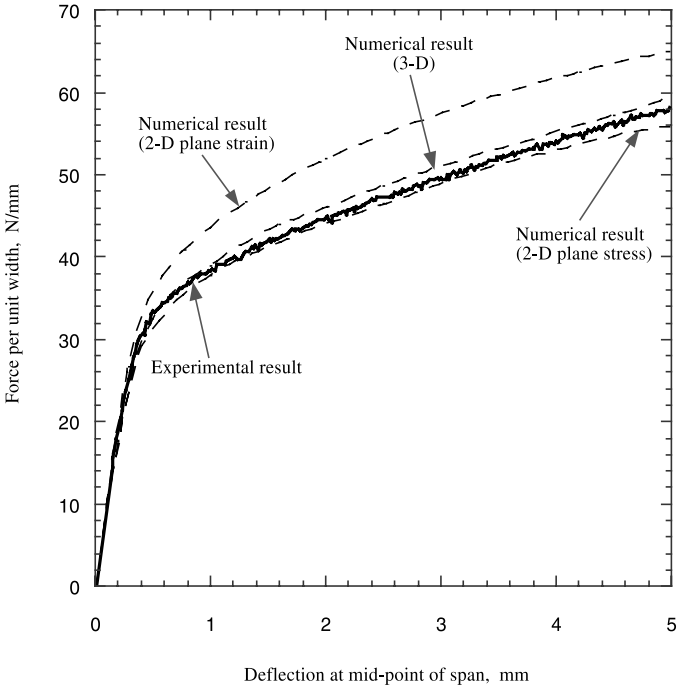

Fig. 10. Numerically predicted and experimentally observed results for the load (per unit width) needed to deform an adhesively bonded beam made with 2.0 mm thick aluminum adherends and tested in three-point bending (with a span of 60 mm between the outside supports). The numerical results were obtained using 2-D plane-stress, 2-D plane-strain and 3-D finite-element elements with a continuum model for the adhesive.

This point is further demonstrated by the force versus deflection curves shown in Fig. 10. In this figure, the experimental results are shown by the solid line. Numerical results of 2-D plane-stress, 2-D plane-strain and 3-D finite-element analyses using a continuum model for the adhesive (not a cohesive-zone model) are also shown in this figure. It is evident that the 2-D plane-stress and 3-D [4] results were in agreement with the experimental data, while the 2-D plane-strain assumption considerably over-estimated the beam stiffness.

References

ABAQUS Finite Element Analysis Code and Technical Manual, Version 5.8., Hibbit, Karlsson and Sorensen, 1998.
Barret, J.D., Foschi, R.O., 1977. Engineering Fracture Mechanics 9, 371–378.
Chai, H., 1988. International Journal of Fracture 37, 137–157.
Chai, H., 1992. International Journal of Fracture 58, 223–239.
Chai, H., 1993. Journal of Materials Science 28, 4944–4956.
Chiang, M.Y.M., Chai, H., 1994. International Journal of Solids and Structures 31, 2477–2490.
Hutchinson, J.W., Evans, A.G., 2000. Mechanics of materials: Top down approaches to fracture, Acta Materialia 48, 125–135.
Hutchinson, J.W., Suo, Z., 1992. Advances in Applied Mechanics 29, 63–191.
Needleman, A., 1987. Journal of Applied Mechanics 54, 525–531.

[4] In this analysis, a relatively coarse mesh was used due to the limited memory size of the computers. Therefore, the 3-D results should be regarded as the upper limit of the actual load–displacement curve.

Needleman, A., 1997. Computational Mechanics 19, 463–469.
Tvergaard, V., Hutchinson, J.W., 1992. Journal of the Mechanics and Physics of Solids 40, 1377–1397.
Tvergaard, V., Hutchinson, J.W., 1993. Journal of the Mechanics and Physics of Solids 41, 1119–1135.
Tvergaard, V., Hutchinson, J.W., 1994. Philosophical Magazine A 70, 641–656.
Wei, Y., Hutchinson, J.W., 1997. Journal of the Mechanics and Physics of Solids 45, 1137–1159.
Wei, Y., Hutchinson, J.W., 1998. International Journal of Fracture 93, 315–333.
Yang, Q.D., Thouless, M.D., Ward, S.M., 1999. Journal of the Mechanics and Physics of Solids 47, 1337–1353.
Yang, Q.D., Thouless, M.D., Ward, S.M., 2000. Journal of Adhesion 72, 115–132.
Yang, Q.D., Thouless, M.D., 2000. International Journal of Fracture, in press.